

# Experimental and numerical investigation of parametric spectral properties of quantum graphs with unitary or symplectic symmetry

Junjie Lu , Jiongning Che , Xiaodong Zhang, and Barbara Dietz \*

*School of Physical Science and Technology, and Key Laboratory for Magnetism and Magnetic Materials of MOE, Lanzhou University, Lanzhou, Gansu 730000, China*



(Received 5 June 2020; accepted 29 July 2020; published 17 August 2020)

We present experimental and numerical results for the parametric fluctuation properties in the spectra of classically chaotic quantum graphs with unitary or symplectic symmetry. A level dynamics is realized by changing the lengths of a few bonds parametrically. The long-range correlations in the spectra reveal at a fixed parameter value deviations from those expected for generic chaotic systems with corresponding universality class. They originate from modes which are confined to individual bonds or explore only a fraction of the quantum graph. Similarly, discrepancies are observed in the avoided-crossing distribution, velocity correlation function, and the curvature distribution of the level dynamics which also may be attributed to such localized modes. We demonstrate that these may be easily identified by inspecting the level dynamics and consequently their nonuniversal contributions to the parametric spectral properties may be diminished considerably. This is corroborated by numerical studies.

DOI: [10.1103/PhysRevE.102.022309](https://doi.org/10.1103/PhysRevE.102.022309)

## I. INTRODUCTION

Quantum graphs [1–4], that is, networks consisting of a finite number of bonds connected at vertices, are used widely to mimic spectral properties of closed and open quantum systems with chaotic classical dynamics [5,6]. They were originally introduced by Linus Pauling to model certain features of organic molecules [7] and are also used for the study of quantum wires [8], optical waveguides and mesoscopic quantum systems [9]. It was proven in Ref. [10] that the spectral properties of closed quantum graphs with incommensurable bond lengths are described by those of random matrices from the Gaussian ensemble [11] of the same universality class [10]. This is in accordance with the Bohigas-Gianonni-Schmit (BGS) conjecture for chaotic systems [12–14].

Quantum graphs have several particular features. First, the semiclassical trace formula, which provides the fluctuating part of the spectral density in terms of a sum over the classical periodic orbits, is exact [2,15]. Second, the correlation functions of scattering matrix elements of open quantum graphs with a classically chaotic scattering dynamics coincide with the corresponding random matrix theory (RMT) results [16–20]. Third, and most importantly, quantum graphs belonging to the orthogonal, the unitary *and* the symplectic universality class can be realized experimentally with microwave networks consisting of coaxial cables connected by joints. Graphs with unitary symmetry correspond to quantum systems without time-reversal ( $\mathcal{T}$ ) invariance, whereas systems belonging to the orthogonal or the symplectic universality class preserve  $\mathcal{T}$  invariance [21–25]. However, in the orthogonal case  $\mathcal{T}^2 = 1$  whereas in the symplectic one  $\mathcal{T}^2 = -1$ , corresponding to integer and half-integer spin systems, respectively [6]. As a consequence, the eigenvalues of GSE

systems exhibit Kramer’s degeneracy. A quantum graph consisting of two coupled GUE graphs that are identical except for a certain phase relation which ensures that it belongs to the symplectic universality class was realized only recently in Ref. [26]. Generic quantum systems with a classically chaotic counterpart which are invariant under  $\mathcal{T}$  operation are described by the Gaussian orthogonal ensemble (GOE) for integer-spin systems with  $\mathcal{T}^2 = 1$  and by the Gaussian symplectic ensemble (GSE) for half-integer spin systems with  $\mathcal{T}^2 = -1$  [6,27], and if time-reversal invariance is violated, by the Gaussian unitary ensemble (GUE).

However, quantum graphs exhibit deviations from RMT predictions [2] which are attributed to backscattering at the vertices of a quantum graph leading to eigenstates which are localized on individual bonds or on a fraction of the graph [28]. Such states were excluded in Refs. [10,17–19] since they are nonuniversal. Deviations are, actually, expected in any quantum system in the long-range correlations of pairs of eigenvalues if their distance is beyond a certain number  $L$  of mean spacings, which is inversely proportional to the length of the shortest periodic orbit [29,30], and observed for example in the number variance  $\Sigma^2(L)$  [11]. It was demonstrated in Ref. [28] that the discrepancies between the experimental or numerical  $\Sigma^2(L)$  statistics of quantum graphs and RMT predictions, observed at a comparatively small value of  $L$ , indeed arise due to the presence of wave functions that are localized on individual bonds. Such modes do not sense the chaoticity of the underlying classical dynamics resulting from the scattering at all vertices. Furthermore, the eigenenergies associated with the localized wave functions depend on the lengths of the associated bonds, and thus are nonuniversal. Unfortunately, the occurrence of such localized modes is unavoidable in microwave networks and the corresponding quantum graphs due to the particular boundary conditions obeyed by the microwaves or wave functions at the ver-

\*dietz@lzu.edu.cn

tices. The effect of these modes on the spectral properties is comparable to that of bouncing-ball orbits in a stadium billiard [30]. However, in distinction to the latter their number is not of measure zero [2]. Consequently, extraction of their contributions to the fluctuating part of the spectral density and thus of their effect on the long-range correlations is not possible.

The subject of the present article are parametric spectral properties of quantum graphs belonging to the unitary and symplectic universality class. The parametric sensitivity of complex systems was investigated theoretically already more than two decades ago in Refs. [31–41]. Furthermore, it was investigated experimentally in flat, normal and superconducting microwave resonators, plates and quartz blocks [42–51]. Parametric GOE graphs were investigated experimentally in Refs. [52,53]. Numerical simulations were performed for GOE and GUE graphs in Refs. [2,54–56]. In both the numerical and the experimental simulations deviations of the avoided-crossing distribution, the curvature distribution and the velocity correlator from the exact RMT results were observed. These were attributed to an insufficient complexity of the graphs. However, we will demonstrate, that the discrepancies dominantly have their origin in the nonuniversal contributions of localized states [55], which are generally present in microwave networks and graphs with Neumann boundary conditions at the vertices so that an increase of the complexity does not necessarily lead to an improvement of the agreement with RMT predictions. We present experimental and numerical results for the parametric spectral properties of GUE and GSE graphs. For these universality classes the extraction of eigenfrequencies from resonance spectra is easier than in the GOE case because they exhibit stronger level repulsion, as explained in Sec. II. The level dynamics of the GUE and GSE quantum graphs is generated by changing the lengths of bonds of the graph, so that nonuniversal contributions can be extracted. Here we use the fact, that eigenstates which are localized on bonds of which the lengths are not changed do not sense the perturbation and, therefore, the associated levels barely depend on the parameter. If an eigenstate is confined to a bond of which the length is changed, the induced perturbation only affects it and thus is local. Furthermore, we propose parametric graphs which do not exhibit effects due to nonuniversal states in the parametric spectral properties.

We will briefly review in Sec. II the salient properties of microwave networks and quantum graphs, introduce the experimental setup and explain how we proceed to determine the eigenvalues of GUE and GSE quantum graphs. In Sec. III we present experimental and numerical results for the spectral properties of the microwave networks and the corresponding quantum graphs. Then, in Sec. IV we present experimental results for the parametric spectral properties of various quantum graphs, and numerical results for several realizations of parametric GUE and GSE graphs. Finally, the results are discussed in Sec. V.

## II. EXPERIMENTAL REALIZATION OF GUE AND GSE QUANTUM GRAPHS WITH MICROWAVE NETWORKS

Quantum graphs consist of  $\mathcal{V}$  vertices that are connected by  $\mathcal{B}$  bonds. The geometry of a graph is defined by the lengths

$L_{ij}$  of the bonds and the connectivity matrix  $\hat{C}$ . Its diagonal entries are  $C_{ii} = 0$  and the off-diagonal ones  $C_{ij}$  equal unity if vertices  $i$  and  $j$  are connected and zero otherwise. Here,  $i, j = 1, \dots, \mathcal{V}$ . The wave-function component  $\psi_{ij}(x)$  on the bond connecting vertices  $i$  and  $j$  are solutions of the one-dimensional Schrödinger equation,

$$-\frac{d^2}{dx^2}\psi_{ij}(x) = k^2\psi_{ij}(x), \quad i, j = 1, \dots, \mathcal{V}, \quad (1)$$

with boundary conditions imposed on  $\psi_{ij}$  at the vertices to ensure continuity and current conservation. To obtain chaotic quantum graphs that can be realized experimentally with microwave networks we chose bonds of incommensurable lengths and Neumann boundary conditions at the vertices.

The microwave networks are constructed from coaxial cables that are connected at  $T$  joints. The cables consist of an inner conductor of radius  $r_1$  and a concentric outer one of radius  $r_2$ . The space between them is filled with Teflon of which the dielectric constant was determined experimentally to  $\epsilon \simeq 2.06$ . For a coaxial cable of length  $L_{ij}$  the optical length is then given as  $L_{ij}^{\text{opt}} = \sqrt{\epsilon}L_{ij}$ . Below the cutoff frequency  $\nu_c = \frac{c}{\pi(r_1+r_2)\sqrt{\epsilon}}$  [57,58] for the first transverse electric mode only the fundamental transverse electromagnetic (TEM) mode can propagate between the conductors. These are the Lecher modes which are described along the coaxial cables by a set of one-dimensional wave equations,

$$\frac{d^2}{dx^2}U_{ij}(x) + \frac{\omega^2\epsilon}{c^2}U_{ij}(x) = 0, \quad i < j, \quad C_{ij} = 1. \quad (2)$$

Here,  $U_{ij}(x)$  denotes the difference between the potentials at the conductors' surfaces,  $c$  is the velocity of light, and  $\omega = 2\pi\nu$  is the angular frequency with  $\nu$  the microwave frequency. This set of equations is also called telegraph equation. It is applicable to lossless coaxial cables, that is, for vanishing Ohmic resistance. At each pair of connected vertices  $i$  and  $j$  the potential difference  $U_{ij}(x)$  obeys the continuity equation,

$$U_{ij}(0) = \phi_i, \quad U_{ij}(L_{ij}) = \phi_j, \quad i < j, \quad (3)$$

and the current is conserved at each vertex,

$$-\sum_{j<i} C_{ij} \left. \frac{d}{dx} U_{ji}(x) \right|_{x=L_{ij}} + \sum_{j>i} C_{ij} \left. \frac{d}{dx} U_{ij}(x) \right|_{x=0} = 0. \quad (4)$$

Equation (2) together with the boundary conditions Eqs. (3) and (4) is mathematically identical to the Schrödinger equation of a quantum graph with Neumann boundary condition at the vertices and bond lengths  $L_{ij}^{\text{opt}}$  [2,4] when identifying  $\sqrt{\epsilon}\omega/c$  of the microwave network with the wave number  $k$  of the quantum graph, implying that the eigenfrequencies of the former yield the eigenvalues of the latter.

The schematic designs of the graphs used for the experimental study of parameter-dependent spectral properties of GUE and GSE graphs are shown in the upper and lower panels of Fig. 1, respectively. In both graphs the valency equals three for all vertices. Time-reversal invariance violation is induced by a  $T$ -shaped circulator [22,25] at vertex 1 (and also  $\bar{1}$  in the GSE graph), which suppresses backscattering and admits a wave entering it at a port to exit it at a certain port only as indicated by the blue arrows, thus leading to unidirectionality of propagation through it.

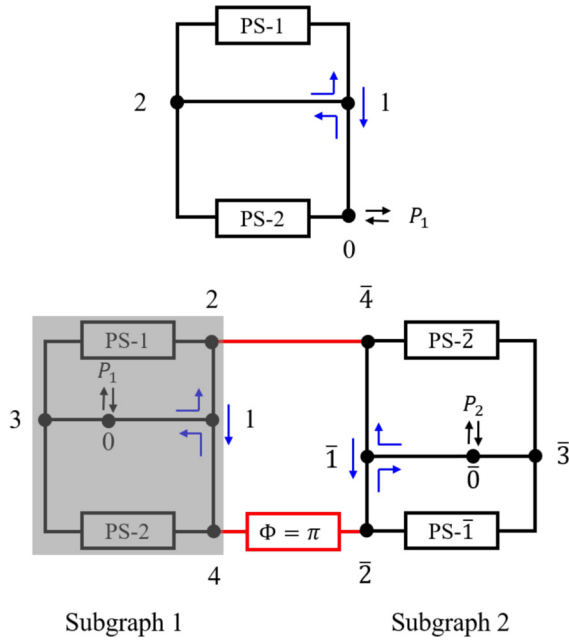


FIG. 1. Schematic view of the quantum graphs used to investigate the spectral properties of quantum systems belonging to the unitary (upper panel) and symplectic (lower panel) universality class, respectively. They consist of vertices of valency three in both cases. Time-reversal invariance violation is induced by replacing  $T$  joints by  $T$ -shaped circulators which induce unidirectionality as indicated by the blue arrows in both panels. The GSE graphs are realized by connecting two subgraphs which are identical except for the orientation of the circulators. Corresponding vertices are marked by  $n$  and  $\bar{n}$ , with  $n = 1, \dots, 4$ . Furthermore, the coaxial cables connecting them have the same length but carry an additional phase of relative size  $\Phi = \pi$ . Parameter-dependent graphs were realized by increasing the length of one coaxial cable and decreasing that of another one by the same amount with phase shifters denoted by PS-1 and PS-2 (PS- $\bar{1}$  and PS- $\bar{2}$ ).

We realized GSE graphs by proceeding as in Ref. [26]. Accordingly, we connected two GUE graphs, which are identical except for the sign of the phase induced by the circulators, by two bonds of same length where the microwaves traveling through one of them experienced an additional phase of size  $\Phi = \pi$ . It was generated by a phase shifter which, actually, changes the length of the coaxial cable by some increment  $\Delta \tilde{l}$  and thus induces a change of the phase accumulated by microwaves passing through it according to the relation

$$\Delta\varphi = k\Delta\tilde{l} = \frac{2\pi\nu}{c}\Delta\tilde{l}, \tag{5}$$

implying that the phase shift  $\Delta\varphi$  depends on the microwave frequency  $\nu$  or wave number  $k = 2\pi\nu/c$ .

A level dynamics, that is continuously changing eigenfrequencies, was realized by varying the lengths of bonds stepwise with a fixed increment  $\Delta l$ . This is achieved by introducing phase shifters, denoted by PS-1, PS-2, PS- $\bar{1}$ , and PS- $\bar{2}$  in Fig. 1. Here, we kept the average spectral density  $\bar{\rho}(k)$ , which is given by Weyl's law,

$$\langle\rho(k)\rangle = \frac{\mathcal{L}}{\pi}, \tag{6}$$

fixed in the experiments by leaving the total length of the network unchanged. Accordingly, we increased the length in one bond stepwise by an increment  $\Delta l$ ,  $\lambda = N\Delta l$  with  $N = 1, 2, \dots, N_{\max}$ , and decreased it in another one by the same amount [2].

The eigenfrequencies of a microwave network are determined experimentally by attaching an antenna to the vertex 0 of the GUE network and to vertices 0 and  $\bar{0}$  for the GSE network and measuring the reflection amplitude  $|S_{00}(\nu)|$  as function of the microwave frequency  $\nu$ . They correspond to the positions  $\nu_i$  of the resonance minima of  $|S_{00}(\nu)|$ . Their identification, generally, is hindered by the broadening of the resonances due to unavoidable absorption of microwave power in the cables,  $T$  joints and circulators. Yet, good agreement between the fluctuation properties in the spectra of quantum systems with a classically chaotic dynamics with those of random matrices belonging to the same universality class is expected only if the eigenvalue sequences are complete [14,25,59]. The problem of absorption was eliminated in experiments with flat, cylindrical microwave resonators simulating quantum billiards [60–63] by performing the measurements with cavities, that are superconducting at liquid-helium temperature [49,51]. This is not possible with microwave networks, because they contain Teflon. Due to broadening, resonances might overlap and thus appear as humps in a broad peak or dip in a transmission and reflection amplitudes, respectively, thereby making the identification of their positions, that is, of the eigenfrequencies, difficult in some cases. In our experiments we took advantage of the measurement of a level dynamics and were able to identify all eigenfrequencies in the frequency range of operation of the circulators by following the evolution of the minima in the reflection spectra as function of the length parameter while varying the lengths in pairs of bonds in such a way that it was increased in one bond and decreased by the same amount in the other one such that the total length was kept constant. Thereby, the average integrated spectral density, i.e., the number of eigenfrequencies  $\langle N(\nu) \rangle = 2\nu\mathcal{L}/c$  below a given frequency  $\nu$  deduced from Eq. (6), did not change. Thus, a jump in  $\langle N(\nu) \rangle$  when comparing the eigenfrequency spectra for two neighboring parameter values might indicate one or more missing levels. These, usually, show up as slight humps in a broad resonance which are difficult to detect otherwise or, in a few cases, are hidden and thus can only be identified by looking at the level dynamics. Based on this procedure we succeeded in extracting complete sequences of eigenfrequencies. The length of the coaxial cables were changed in steps of size  $\Delta l = 0.84$  mm. The total length of the GUE graph was  $\mathcal{L} = 2.60$  m, that of the GSE graph equaled  $\mathcal{L} = 6.68$  m, and the lengths was varied in  $N_{\max} = 60$  steps in the former one and in  $N_{\max} = 43$  steps in the latter one, corresponding to a maximal change of the respective bond length by about 1–2% of  $\mathcal{L}$ . An example is shown in Fig. 2.

In the experiments with the GSE graphs we attached a second antenna at the vertex  $\bar{0}$  and measured in addition to  $|S_{00}(\nu)| = 0$  transmission amplitudes  $|S_{0\bar{0}}(\nu)|$  and  $|S_{\bar{0}0}(\nu)|$  to achieve a more accurate tuning of the relative phase of microwaves traveling through both connecting bonds to  $\Phi = \pi$  than is possible with the phase shifters which give  $\Delta\varphi$  with a certain error. Here, we exploited the fact that transmission

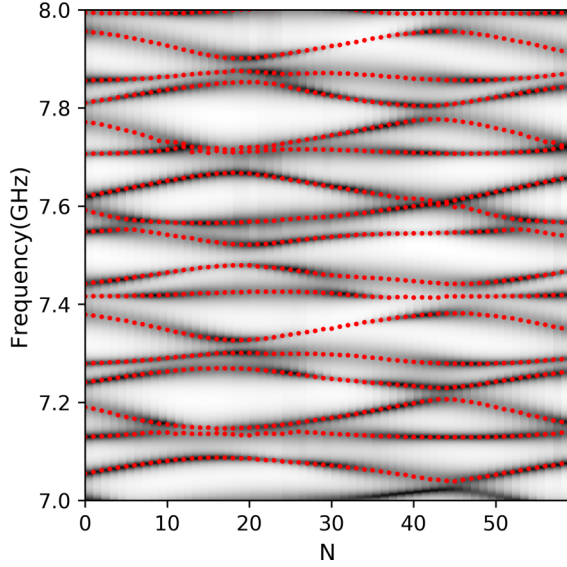


FIG. 2. Reflection spectrum  $S_{00}$  of the GUE microwave network (gray scale varying from black ( $|S_{00}(\nu)| = 0$ ) to white ( $|S_{00}(\nu)| = 1$ ) as function of the length change caused by the phaser PS-1 in Fig. 1, i.e., of the number of steps  $N$  of size  $\Delta l$ . Complete sequences of eigenfrequencies (red [gray] dots) were obtained by following the evolution of the minima in the reflection spectra.

is suppressed for a phase shift  $\Phi = \pi$  since the microwaves traveling through both connecting bonds from port 0 to port  $\bar{0}$  then interfere destructively at port  $\bar{0}$ . This is illustrated in Fig. 3. In Fig. 4 we show in a density plot the transmission amplitudes  $|S_{0\bar{0}}(\nu)|$  as function of frequency  $\nu$  versus the length increase  $\Delta \bar{l}$  (top) and the thereby induced phase change  $\Delta \varphi$  (bottom) of the bond connecting vertices 4 and  $\bar{2}$  in Fig. 1.

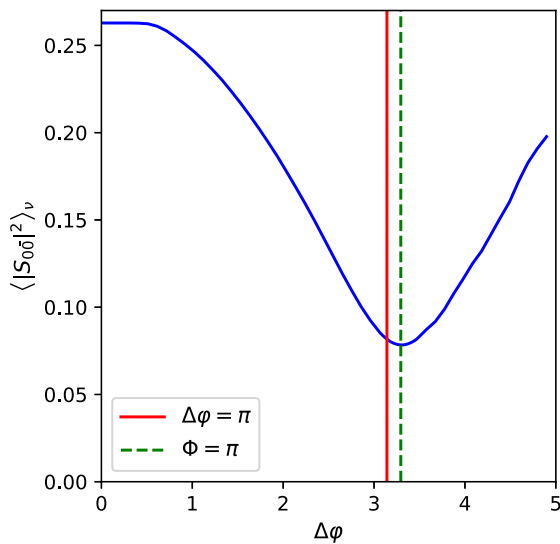


FIG. 3. Average transmission amplitude  $\langle |S_{0\bar{0}}(\nu)|^2 \rangle_\nu$  as function of the phase shift  $\Delta \varphi$  read off the phase shifter. The relative phase of  $\Phi = \pi$  experienced by microwaves traveling through the connecting bonds and required to realize a GSE graph, is identified as the phase shift yielding a minimal  $\langle |S_{0\bar{0}}(\nu)|^2 \rangle_\nu$ .

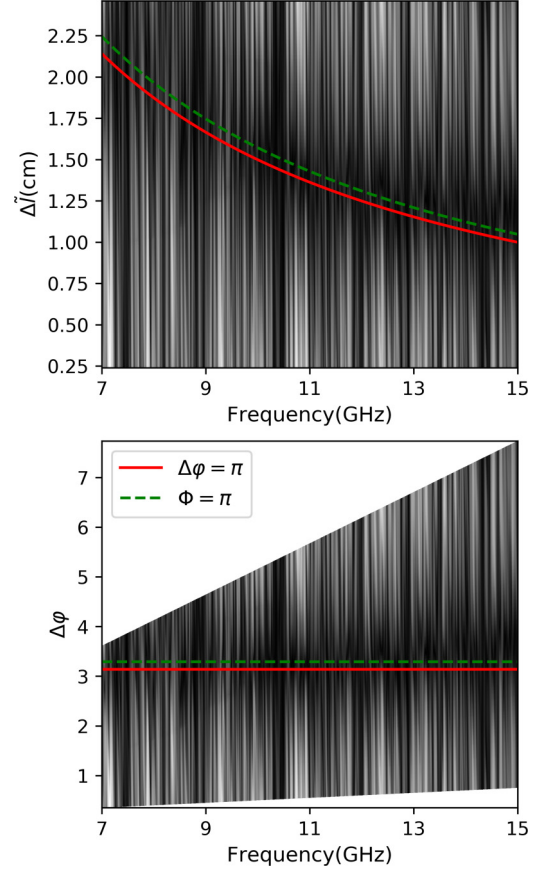


FIG. 4. Density plot of the transmission amplitude  $|S_{0\bar{0}}(\nu)|$  versus microwave frequency  $\nu$  for fixed relative length differences  $\Delta \bar{l}$  (top) and relative phase shift  $\Delta \varphi$  (bottom) between the bonds connecting vertices 2 and  $\bar{4}$ , respectively, 4 and  $\bar{2}$ .

To corroborate our experimental results we also performed numerical simulations with GUE and GSE quantum graphs. The microwave networks were designed such that the effect of absorption was minimized by choosing the number of coaxial cables as small as possible to achieve GUE or GSE behavior of the spectral properties. Accordingly, the experimental GUE and GSE networks consisted of 3 vertices and 4 bonds, and of two copies with 5 vertices and 7 bonds including the connecting bonds, respectively. To demonstrate, that these numbers are sufficient we compared with numerical results for more complex graphs, which consisted of 12 vertices and 20 bonds for the GUE graph, and two copies with 7 vertices and 10 bonds for the GSE graph. The lengths of the bonds were chosen similar to those of the coaxial cables and increased or decreased stepwise by the same increment  $\Delta l = 0.84$  mm. We computed approximately 500 eigenfrequencies in all numerical simulations for 100 parameter values were the maximal change of length  $\lambda = N_{\max} \Delta l$  of a bond was approximately 3% of  $\mathcal{L}$ .

The directionality induced in the experiments by the circulators can not be accounted for in the vertex secular equation deduced from the quantization condition for closed quantum graphs [2]. In previous theoretical studies of GUE and GSE graphs [25,26] their effect was modelled by introducing a phase  $A_{ij} = -A_{ji} = \pi/2$  on the bonds connected to the

circulator. Furthermore, in the experiments the graphs are slightly opened by attaching antennas. This is equivalent to attaching leads to the corresponding vertices of the quantum graphs that are extended to infinity. Thus, to obtain a description which is as close as possible to the experimental situation, we determined the reflection and transmission amplitudes of open quantum graphs based on the bond scattering matrix  $\hat{S}_B(k; \{\Phi_{ij}\})$  [4,64] and the eigenvalues of closed ones from the associated secular equation

$$\zeta_B(k) = \det[1 - \hat{S}_B(k; \{\Phi_{ij}\})] = 0. \quad (7)$$

For a quantum graph with  $\mathcal{B}$  bonds the bond scattering matrix is a  $2\mathcal{B} \times 2\mathcal{B}$  matrix,  $\hat{S}_B(k; \{\Phi_{ij}\}) = \hat{D}(k; \{\Phi_{ij}\})\hat{T}$  in the  $2\mathcal{B}$  space of directed bonds,

$$\hat{D}_{ij, nm} = \delta_{i,n}\delta_{j,m}e^{ikL_{ij} + \Phi_{ij}}, \quad \hat{T}_{ji, nm} = \delta_{n,i}C_{j,i}C_{n,m}\hat{\sigma}_{ji, nm}^{(i)}, \quad (8)$$

where the relative phase of  $\pi$  is accounted for in the phases  $\Phi_{ij}$  and the directionality at the circulators is incorporated in the transition matrix  $\hat{T}_{ji, im}$  from vertex  $m$  to vertex  $j$  via vertex  $i$ , with  $i = 1, \bar{1}$  in Fig. 1. The vertex scattering matrix  $\hat{\sigma}^{(i)}$  equals  $\hat{\sigma}_{ji, im}^{(i)} = (\frac{2}{3} - \delta_{jm})$  at the  $T$  joints, whereas at the circulator at vertex 1 ( $\bar{1}$ ) it is given by

$$\hat{\sigma}^{(1)} = \begin{pmatrix} 0 & 0 & 1 \\ 1 & 0 & 0 \\ 0 & 1 & 0 \end{pmatrix}, \quad (9)$$

when marking its ports clockwise (counterclockwise) by 1, 2, and 3, respectively. The solutions of Eq. (7) yield the eigenvalues of a closed quantum graph.

The microwave networks were constructed from microwave coaxial cables (HASCO SMA-RG402), which have a cut-off frequency  $\nu_c \simeq 33$  GHz and  $T$ -joints (Pomona Electronics 72968). Time-reversal invariance violation was induced with circulators (Pasternack PE8403) which function in the frequency interval 7–15 GHz. To change the lengths of coaxial cables or realize a phase difference of  $\Phi = \pi$  between the cables connecting the copies of GUE graphs in the GSE graph, we used phase shifters (ATM P1507D). For the measurement of the reflection and transmission amplitudes we attached antennas to the ports denoted “0” and “ $\bar{0}$ ” in Fig. 1 and connected them to a vector network analyzer (Keysight N5227A) via coaxial cables.

### III. FLUCTUATION PROPERTIES IN THE EIGENFREQUENCY SPECTRA OF THE MICROWAVE NETWORKS

Before comparing the spectral properties of quantum systems with a chaotic classical counterpart with random matrix theory (RMT) predictions, their system-specific properties need to be eliminated by unfolding the eigenvalues such that the spectral density is uniform, that is, the mean spacing is constant across the whole spectrum. Quantum graphs and microwave networks have the advantage, that the mean spectral density, which is given by Weyl’s law Eq. (6) is frequency independent. Accordingly, the unfolded eigenvalues  $\epsilon_i$  of mean spacing unity are easily obtained from the ordered eigenfrequencies  $\nu_i$ ,  $\nu_{i+1} \geq \nu_i$ ,  $i = 1, 2, \dots$  as  $\epsilon_i = 2\nu_i\mathcal{L}/c$ . The experimentally obtained dynamics of the unfolded eigenvalues

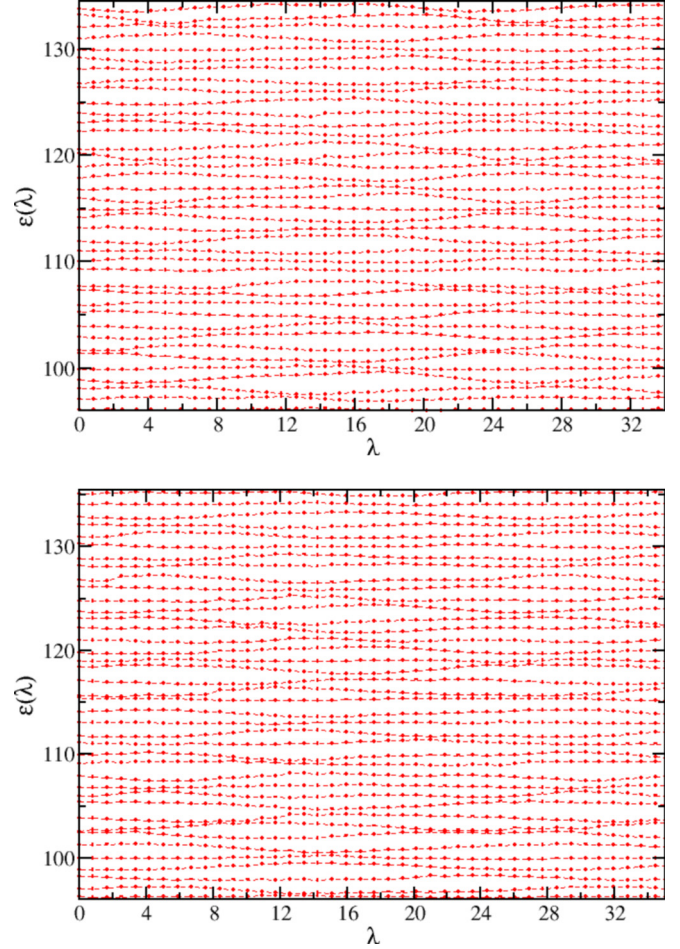


FIG. 5. Level dynamics obtained from the experimental reflection spectra of the microwave networks with unitary (upper panel) and symplectic (lower panel) symmetry shown schematically in Fig. 1. Here,  $\lambda$  corresponds to the absolute value of the change in length  $\lambda = N\Delta l$ ,  $N = 1, \dots, N_{\max}$  induced in bonds comprising a phaser.

of the microwave networks sketched in Fig. 1 is depicted in Fig. 5 for the GUE graph (top) and GSE graph (bottom).

We first investigated fluctuation properties in the eigenvalue spectra for fixed  $\lambda$  to test whether they comply with the prediction of the BGS conjecture, that is, behave like typical chaotic systems with corresponding universality class. In Fig. 6 we show the nearest-neighbor spacing distribution  $P(s)$  of adjacent spacings  $s_i = \epsilon_{i+1} - \epsilon_i$  which provides a measure for short range correlations. Furthermore, we show as a representative for long-range correlations the variance  $\Sigma^2(L) = \langle (N(L) - \langle N(L) \rangle)^2 \rangle$  of the number of unfolded eigenvalues  $N(L)$  in an interval of length  $L$ , where  $\langle N(L) \rangle = L$  for a proper unfolding procedure. The  $\Sigma^2(L)$  statistics is particularly sensitive to missing levels and to contributions which are nongeneric in the sense that they do not comply with the BGS conjecture for typical chaotic systems with corresponding universality class. Shown are the results obtained from the experimental eigenfrequencies (black histograms and triangles up) of the microwave networks shown schematically in Fig. 1, those for the numerically computed eigenvalues of quantum

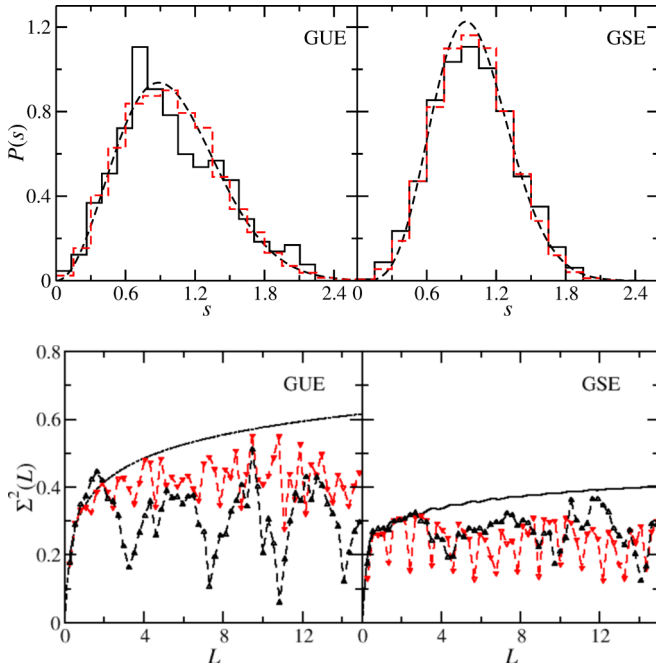


FIG. 6. Nearest-neighbor spacing distribution  $P(s)$  (upper panels) and number variance  $\Sigma^2(L)$  (lower panels). The black curves and triangles up show the results obtained from measurements with the microwave networks shown schematically in Fig. 1 for the GUE (left panels) and GSE (right panels) universality classes. The red (gray) dashed curves and triangles down were obtained from numerical simulations of GUE and GSE quantum graphs. The corresponding RMT curves are shown as black dashed lines.

graphs (red [gray] histograms and triangles down) belonging to the unitary (left) and symplectic (right) universality class and the corresponding RMT curves (black dashed lines). Note that even though the microwave networks are constructed from a small number of bonds and vertices, the experimental curves are close to the numerical results for the more complex quantum graphs.

For the nearest-neighbor spacing distribution agreement of the experimental curve with the numerical and RMT curves is good except in the region around the peak in the GUE case. These deviations may be attributed to the

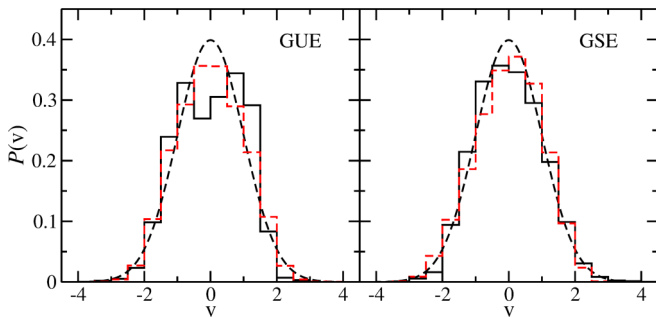


FIG. 7. Velocity distributions of GUE (left) and GSE (right) graphs. Compared are the experimental (black histograms) and corresponding numerical results (red [gray] dashed-line histograms) with the associated RMT curve (dashed line).

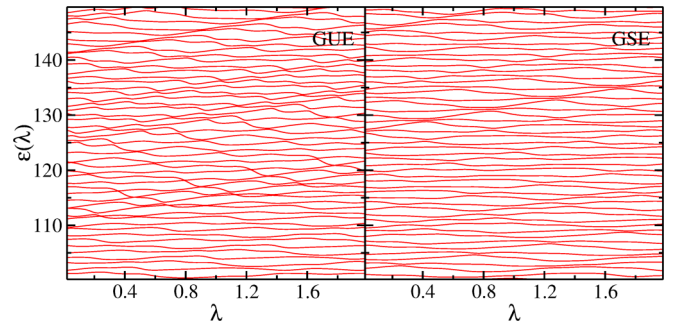


FIG. 8. Numerically computed level dynamics of a GUE (left) and GSE (right) graph. In the former the length of one bond was increased by  $\lambda$ , in the latter those of two corresponding bonds were increased by  $\lambda$ .

experimental inaccuracy in the determination of the eigenfrequencies. Nevertheless, the results confirm that the microwave networks indeed belong to the unitary and symplectic universality class, respectively. For the  $\Sigma^2(L)$  statistics we find good agreement between the experimental, numerical and RMT results only below  $L \simeq 2 - 3$ , and thus recover the findings of Ref. [28]. There, the discrepancies beyond a certain value of  $L$  were attributed to the occurrence of short periodic orbits confined to individual bonds by backscattering at the vertices bordering them. These orbits do not sense the chaoticity of the classical dynamics associated with the quantum graph, which arises due to the scattering of the wave functions—or of the microwaves in the experiments—at all its vertices. In addition, they depend on the lengths of the associated bonds, as is clearly visible in the periods of the oscillations of the experimental and numerical curves, and thus lead to nonuniversal features of the spectral properties. Since the number of periodic orbits that travel only through a fraction of the quantum graph is large [2], it is impossible to extract their contributions from the eigenvalue spectra. However, as will be outlined in the following section, it is possible to diminish their effect on parametric spectral properties.

Note, that the nearest-neighbor spacing distributions increase around  $s \simeq 0$  as  $P(s) \simeq s^2$  and  $P(s) \simeq s^4$  for the GUE and GSE, respectively, implying that the probability that two eigenfrequencies are close to each other is low for the GUE graph and much smaller for the GSE graph. This

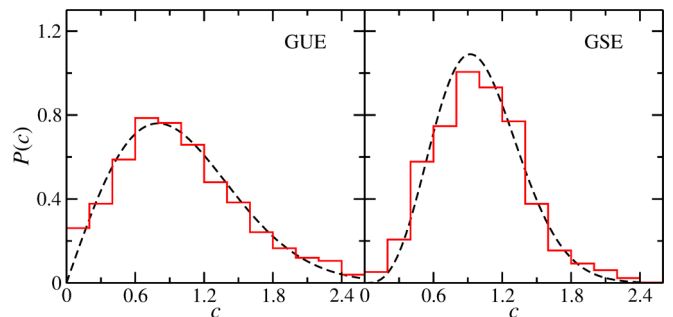


FIG. 9. Comparison of the avoided-crossing distribution of the level dynamics (red [gray] curves) shown in Fig. 8 with the RMT result (black dashed line).

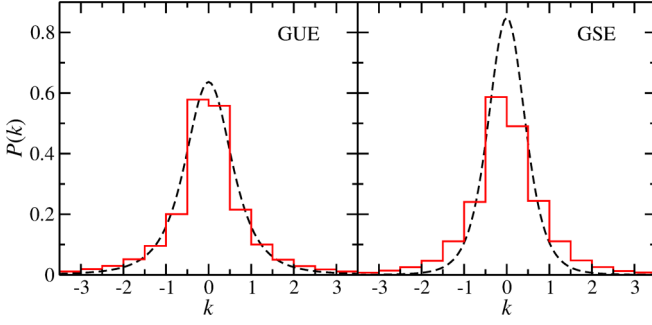


FIG. 10. Comparison of the curvature distribution of the level dynamics (red [gray] curves) shown in Fig. 8 with the RMT result (black dashed line).

characteristics is of particular advantage for the identification procedure of the eigenfrequencies of microwave networks.

#### IV. PARAMETRIC FLUCTUATION PROPERTIES OF THE LEVEL DYNAMICS

In this section we investigate the spectral properties of the parameter-dependent unfolded eigenfrequencies  $\epsilon_i(\lambda)$  of the family of graphs generated by varying the lengths  $L_{ij}$  of two or four coaxial cables (see Fig. 1) in the experiment or of some bonds in the numerical simulations, of which the number will be further specified in the corresponding subsection. They were changed stepwise by an increment  $\Delta l$ ,  $\tilde{L}_{ij} = L_{ij} + \lambda$ ,  $\lambda = N\Delta l$ ,  $N = 1, \dots, N_{\max}$ . The specific form of the parameter  $X$  which thereby induces a transformation of the quantum graph is not needed, because for the characterization of universal parametric properties system-specific properties have to be extracted. System-specific properties become manifest in the variance  $\sigma_X$  of the velocities  $\partial\epsilon_i(X)/\partial X$  [65],

$$\sigma_X^2 = \frac{1}{N} \sum_{j=1}^N \left( \frac{\partial\epsilon_i(X)}{\partial X} - \left\langle \frac{\partial\epsilon_i(X)}{\partial X} \right\rangle \right)^2, \quad (10)$$

where the average  $\langle \partial\epsilon_i(X)/\partial X \rangle \simeq 0$  in the systems considered in the present article. The system-specific properties related to the parametric variation are eliminated by unfolding not only the eigenfrequencies for a fixed parameter value  $X$  but also the parameter along each curve  $\epsilon_i(X)$ . We applied two unfolding

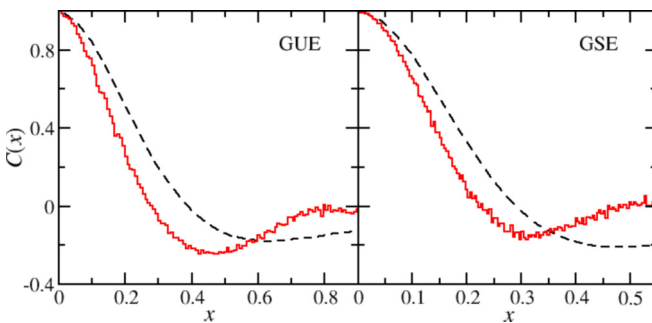


FIG. 11. Comparison of the velocity-correlation function of the level dynamics (red [gray] curves) shown in Fig. 8 with the RMT result (black dashed line).

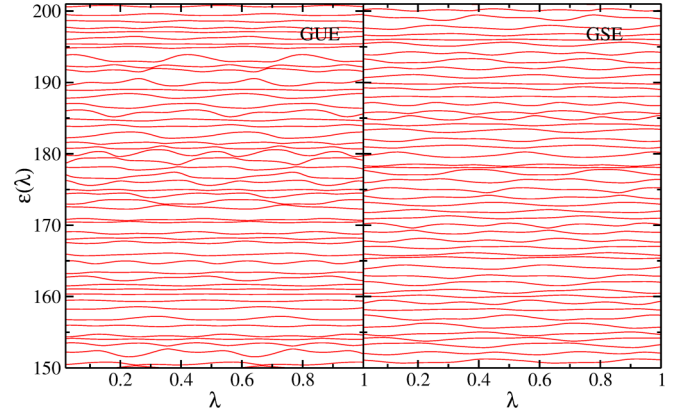


FIG. 12. Numerically computed level dynamics of a GUE (left) and GSE (right) quantum graph. The lengths of two bonds were changed in the GUE graph and identically in each copy of the GSE graph such that the total length was unchanged. Thus, the spectral density is independent of the parameter.

procedures to the parameter  $X$ ,

$$\Lambda = \sigma_X X \quad (11)$$

and

$$\Lambda = \int_0^X \sigma_{X'} dX'. \quad (12)$$

Both procedures yield similar results. This may be attributed to the fact that the lengths of the bonds are varied linearly. Accordingly, we present only results which were obtained on the basis of the unfolding procedure Eq. (11). For fully chaotic systems, the velocities should be Gaussian distributed with variance unity independently of the universality class if the unfolding procedure is applied properly. We compare in Fig. 7 the distributions obtained from the experiments (black histogram) and corresponding numerical simulations (red [gray] dashed histogram) with the RMT curve (black dashed line). Similar results were obtained for the other realizations of parametric quantum graphs.

We considered three statistical measures for the spectral properties of the level dynamics, the distribution of avoided crossings  $P(c)$ , where  $c$  is the distance between two neighboring eigenvalues  $\epsilon_i(\Lambda)$  and  $\epsilon_{i+1}(\Lambda)$  at closest encounters, the

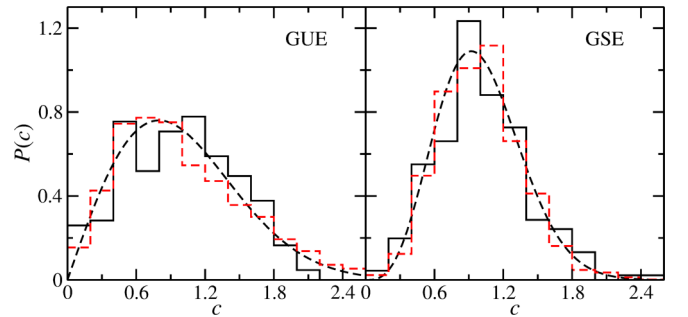


FIG. 13. Comparison of the avoided-crossing distribution of the experimental (black lines) and numerical level dynamics (red [gray] dashed lines) shown in Figs. 5 and 12, respectively, with the RMT result (black dashed line).

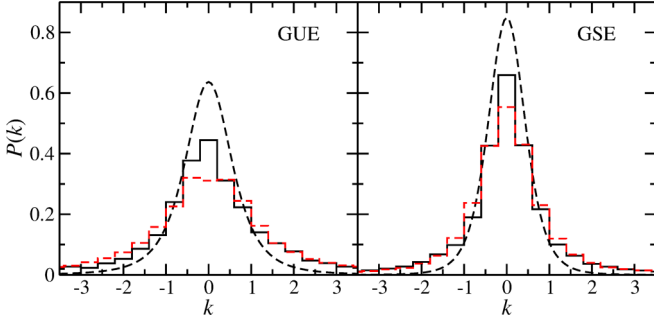


FIG. 14. Comparison of the curvature distribution of the experimental (black lines) and numerical level dynamics (red [gray] dashed lines) shown in Figs. 5 and 12, respectively, with the RMT result (black dashed line).

distribution of the curvatures  $k_j$ ,

$$k_j = \frac{1}{\pi\beta} \frac{\partial^2 \epsilon_j(\Lambda)}{\partial^2 \Lambda}, \quad (13)$$

and the velocity-correlation function,

$$C(x) = \left\langle \frac{\partial \epsilon_j(\Lambda)}{\partial \Lambda} \Big|_{\Lambda=\Lambda_0} \frac{\partial \epsilon_j(\Lambda)}{\partial \Lambda} \Big|_{\Lambda=\Lambda_0+x} \right\rangle_{\Lambda_0, j}. \quad (14)$$

Analytical expressions were derived for all three Gaussian ensembles for the avoided-crossing distribution  $P(c)$  [31,32],

$$P^{\beta=2}(c) = \frac{\pi}{2} c \exp\left(-\frac{\pi}{4} c^2\right), \quad (15)$$

$$P^{\beta=4}(c) = \frac{81\pi^2}{128} c^3 \exp\left(-\frac{9\pi}{16} c^2\right),$$

and the curvature distribution  $P(k)$  [33,37–39],

$$P^{\beta=2}(k) = \frac{2}{\pi} \frac{1}{(1+k^2)^2}, \quad (16)$$

$$P^{\beta=4}(k) = \frac{8}{3\pi} \frac{1}{(1+k^2)^3},$$

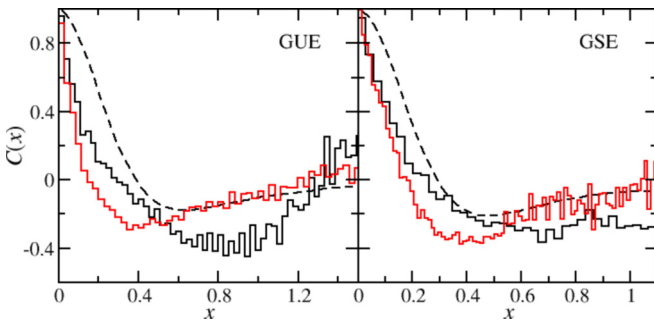


FIG. 15. Comparison of the velocity-correlation function of the experimental (black lines) and numerical level dynamics (red [gray] lines) shown in Figs. 5 and 12, respectively, with the RMT result (black dashed line).

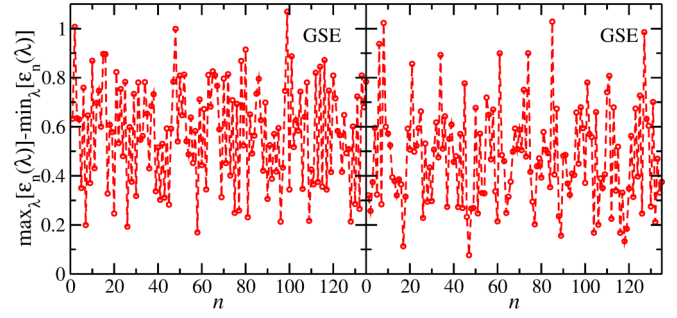


FIG. 16. Difference between the maximal and minimal value of each eigenvalue  $\epsilon_n(\lambda)$  as function of  $n$ .

whereas for the velocity correlator only the asymptotic behavior is known for large  $x$ ,

$$C(x) \rightarrow -\frac{2}{\beta x^2}, \quad x \gg 1, \quad (17)$$

and for  $\beta = 2, 4$  [34,35,40] for small  $x \ll 1$ , respectively,

$$C^{\beta=2}(x) \simeq 1 - 2x^2, \quad (18)$$

$$C^{\beta=4}(x) \simeq 1 - \frac{8}{3}x^2.$$

In the following three subsections we summarize our experimental and numerical results for different level dynamics which were generated by varying the number of bonds of which the lengths were varied.

### A. Increasing the lengths of bonds

Before doing the experiments we performed various numerical simulations to design the microwave networks. First, we performed parametric variations by increasing the length of only one bond in the GUE graph and of two corresponding ones in the GSE graph. Accordingly, the average integrated spectral density  $\langle N(k) \rangle = k\mathcal{L}/\pi$  increases linearly with  $\lambda = N\Delta l$  [53]. The resulting level dynamics is shown in Fig. 8 for the GUE (left panel) and the GSE (right panel) graph. Figures 9–11 display the numerical (red [gray] curves) and RMT results (black dashed lines) for the avoided-crossing and curvature distributions and the velocity correlators for the GUE (left panels) and the GSE (right panels) graphs,

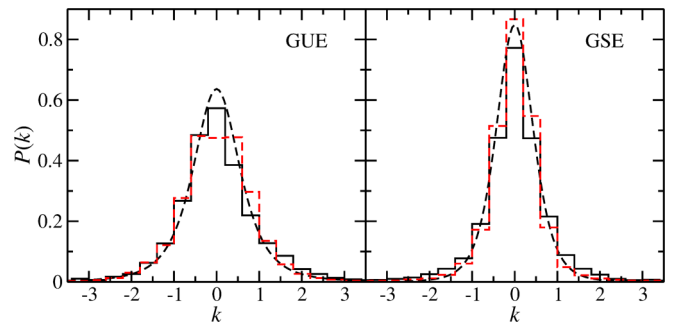


FIG. 17. Same as described in the caption of Fig. 14 after cutting out energy levels corresponding to wave functions trapped on individual bonds.

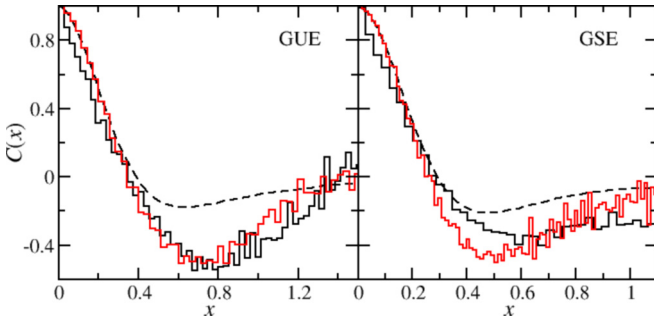


FIG. 18. Same as described in the caption of Fig. 15 after cutting out energy levels corresponding to wave functions trapped on individual bonds.

respectively. Deviations are clearly visible in the curvature distribution for the GSE graph and for both universality classes in the velocity correlator. The latter results are similar to those obtained for microwave networks belonging to the GOE and numerically also for GUE quantum graphs in Refs. [2,52–54]. As already assumed in these works, we attribute these deviations to the presence of nonuniversal features resulting from wave functions confined to individual bonds or a fraction of the graph due to backscattering at the vertices. The corresponding unfolded eigenfrequencies are recognizable as stripes of nonzero slope formed by adjacent ones in Fig. 8. Indeed, the eigenfrequencies associated with such localized states depend weakly on the parameter, when they are localized on bonds of which the lengths are not changed, or else only the localized state is affected by the perturbation, which thus is local, so that their velocities are vanishingly small and change linearly with the length after unfolding. To eliminate their effect on the spectral properties of the level dynamics shown in Fig. 8 we would need to disregard the stripes, that is, cut out the corresponding eigenvalues from the sequence of spectra, which can be tedious [41,66].

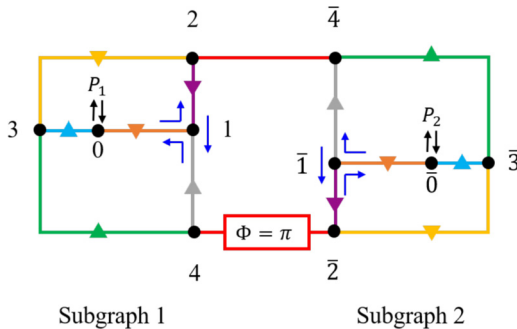


FIG. 19. Schematic view of the GSE quantum graph used to numerically investigate the parametric spectral properties for an increasing number of pairs of bonds of which the length were varied. In bonds marked by triangle up the lengths was increased in steps by an increment  $\Delta l$ , and simultaneously it was decreased in the bonds marked by triangles down. In the first simulation we varied the lengths of the green  $[(3, 4), (\bar{3}, \bar{4})]$  and yellow  $[(2, 3), (\bar{2}, \bar{3})]$  bonds, in the second in addition those of the cyan  $[(0, 3), (\bar{0}, \bar{3})]$  and orange  $[(0, 1), (\bar{0}, \bar{1})]$  bonds and, finally, also those of the gray  $[(1, 4), (\bar{1}, \bar{4})]$  and violet  $[(1, 2), (\bar{1}, \bar{2})]$  ones.

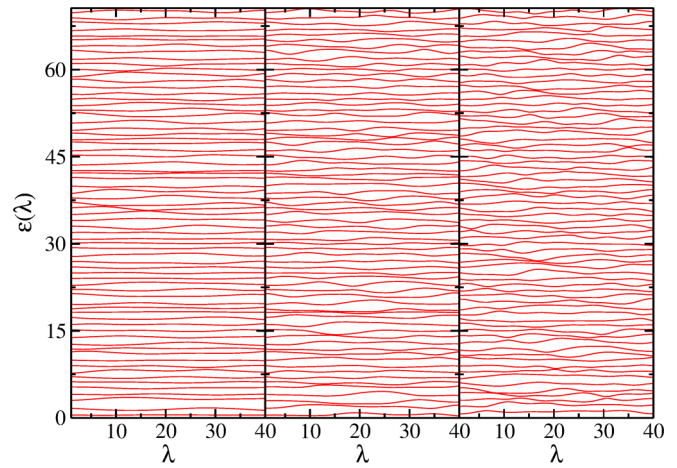


FIG. 20. Level dynamics of the GSE graph shown schematically in Fig. 19, where the lengths of in total two (left panel), four (middle panel) and six (right panel) bonds were changed in each of its halves.

We, instead considered a different parametric variation, where the lengths of two bonds were varied such that the integrated spectral density remained constant [2].

### B. Variation of the lengths of pairs of bonds, keeping $\langle N(k) \rangle$ unchanged

Figures 5 and 12 show the experimental and numerical level dynamics for GUE (upper panel) and GSE (lower panel) graphs. They were generated by varying the lengths of pairs of bonds in such a way that the total length of the graph was unchanged. The experimental (black full lines) and numerical (red [gray] lines) results for the associated avoided-crossing and curvature distributions and the velocity correlator are shown in Figs. 13–15. The experimental and numerical results are similar, even though we chose more complex quantum graphs for the latter. However, while agreement of them with the RMT results (black dashed lines) is comparatively good for the avoided crossings [49,67,68], this is not the case for the curvature distribution and the velocity correlator. These deviations are again attributed to the effect of wave functions which are confined to bonds of nonvarying length and thus are associated with eigenvalues of velocity zero in the level dynamics. Since the spectral density, and thus the unfolding do not change with the parameter, they can be easily identified as nearly straight lines of slope zero. In Fig. 5 examples are the eigenvalues starting at  $\epsilon(\lambda = 0) \simeq 109$  for the GUE graph (upper panel) and at  $\epsilon(\lambda = 0) \simeq 114$  for the GSE graph (lower panel). Similarly, the eigenvalues close to  $\epsilon(\lambda) \simeq 188$  in the left panel and  $\epsilon(\lambda) \simeq 190$  in the right one of Fig. 12 are examples for the numerical GUE and GSE graph, respectively. To identify such “trivial” eigenvalues, we computed for each eigenvalue  $\epsilon_n(\lambda)$  the difference between its maximal and minimal value in the considered  $\lambda$  range,  $\delta(\lambda) = \max_{\lambda}[\epsilon_n(\lambda)] - \min_{\lambda}[\epsilon_n(\lambda)]$ . Examples are shown in Fig. 16 where  $\delta(\lambda)$  is plotted for the experimental (left) and numerical (right) GSE graph. To extract nonuniversal contributions, we discarded those  $\epsilon_n(\lambda)$ , for which  $\delta(\lambda)$  was below a certain threshold, which was one quarter of the mean spacing in Figs. 17 and 18. The agreement between the

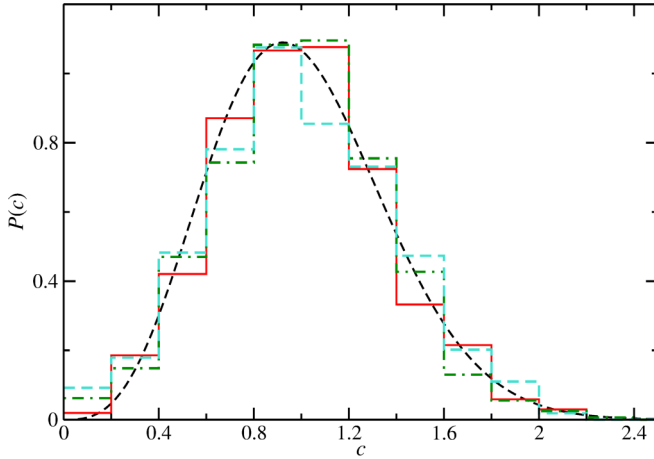


FIG. 21. Comparison of the avoided-crossing distribution obtained for the level dynamics shown in Fig. 19 with the RMT result (black dashed line). The red (gray) curve is obtained for the case of in total four varying lengths, the green one (dash-dotted line) for that of eight varying lengths and the turquoise one (dashed line) when changing the lengths of all bonds.

experimental, respectively, the numerical curvature distributions and velocity correlators and the RMT results improves, in the latter case for  $x$  below its value at the minimum of  $C(x)$ . To obtain an estimate for the improvement we fit a function to the experimental and numerical curvature distributions,  $P^\beta(k) = \mathcal{N}_\beta / (1 + k^2)^\alpha$ , where  $\mathcal{N}_\beta$  is the normalization and  $\alpha = (2 + \beta)/2$  serves as fit parameter. For  $\beta = 2, 4$ , i.e.,  $\alpha = 2, 3$  it coincides with the analytical results Eq. (16) for the unitary and symplectic cases. The fit yielded for the experimental GUE and GSE graphs before cutting out nonuniversal contributions  $\alpha = 1.2$  and  $\alpha = 1.7$ , and afterwards  $\alpha = 1.7$  and  $\alpha = 2.9$  which are close to the expected values (see Eq. (16)). The results were similar for the numerical ones. This finding confirms our assumption that deviations may be attributed to the effect of localized states. To take into account all levels associated with wave functions which are localized on a small fraction of the graph, the threshold for  $\delta(\lambda)$  would have to be increased. However, then the set of available data, and thus their statistical relevance, would decrease which is an important issue for the experimental data. Thus, at this point, the fact that we use simple microwave networks with minimally required complexity becomes perceptible.

**C. Variation of the lengths of an increasing number of bonds, keeping  $\langle N(k) \rangle$  unchanged**

To further verify this assumption we performed additional numerical simulations with GSE graphs, where we added successively phasers to corresponding bonds, that is, changed lengths in an increasing number of such pairs, as illustrated in Fig. 19. First we considered a graph where the lengths of the two bonds connecting vertices  $(3,4)$   $(\bar{3}, \bar{4})$  (green, triangle up) were increased and two other ones  $[(2, 3), (\bar{2}, \bar{3})]$  (yellow, triangle down) were decreased, then we, in addition, increased the lengths of two further bonds  $[(0, 3), (\bar{0}, \bar{3})]$  (cyan, triangle up) and decreased those by the same amount in two other ones  $[(0, 1), (\bar{0}, \bar{1})]$  (orange, triangle down), were the

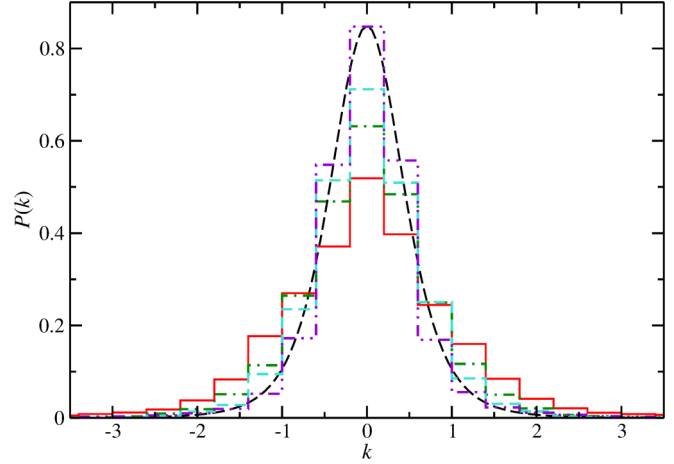


FIG. 22. Same as described in the caption of Fig. 21 for the curvature distribution. In addition, we show the result for the case where the length increment was chosen differently for each quadruplet of bonds as violet dash-dotted-dotted line.

length increment was chosen equal in all bonds. Finally, we increased lengths in the green, cyan and gray-colored bonds  $[(1, 4), (\bar{1}, \bar{4})]$  and decreased them by the same amount in the yellow, orange and violet coloured bonds  $[(1, 2), (\bar{1}, \bar{2})]$ . The resulting level dynamics are shown in Fig. 20. For the case, where the lengths of only two bonds (left panel) were varied in each half of the GSE graph, which corresponds to the experimental situation, eigenvalues corresponding to wave functions which are localized on the unchanged bonds, and thus barely depend on  $\lambda$  are clearly visible as nearly-straight lines. With increasing number of bonds of which the lengths were varied, their number decreases. Accordingly, this provides a method with which nongeneric effects may be extracted. This is reflected in the curvature distribution and the velocity correlator which are shown in Figs. 21–23. While the avoided-crossing distribution barely changes with increasing number of bonds of which the length is varied, agreement between the RMT result (black dashed line) and the numerical one shown as full red (gray) line, dash-dotted

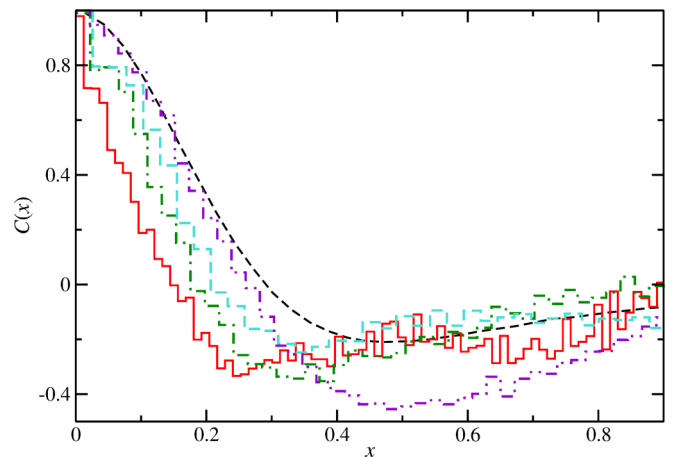


FIG. 23. Same as described in the caption of Fig. 22 for the velocity correlator.

green line and dashed turquoise line for in total four, eight and twelve bonds of which the lengths are varied improves with the number of varied bonds. The agreement between the RMT and numerical curves becomes good for the more complex GSE graph used for the numerical simulations in the previous subsections, when varying all bond lengths while keeping the resonance density unchanged. Furthermore, we chose the increments for each quadruplet of bonds of constant total length differently thus achieving a higher complexity. The results are shown as violet (dash-dotted-dotted line) curves in Figs. 22 and 23. A fit to  $P^\beta(k) = \mathcal{N}_\beta / (1 + k^2)^\alpha$  yielded  $\alpha = 1.4, 1.9, 2.3, 3.0$  for the cases where the lengths of four, eight, twelve and fourteen bonds were varied, thus confirming our observation that in the latter case agreement with the RMT results is good. This corroborates our assumption that the discrepancies between the parametric spectral properties of a quantum graph and RMT have their origin in the presence of localized wave functions, as was proposed for GOE graphs in Ref. [55].

## V. CONCLUSIONS

We investigated experimentally and numerically parametric fluctuation properties in the spectra of microwave networks simulating quantum graphs belonging to the unitary or symplectic universality class. Here, the parametric variations of the eigenvalues were realized by varying the lengths of bonds of the graph, while keeping its total length and thus the spectral density fixed. As in the parameter-independent case the spectral properties deviate from RMT predictions. Similar observations were made in previous experiments with GOE graphs [52,53] and attributed to insufficient complexity of the graphs, that is, to a too small number of vertices. We,

however, demonstrate that the deviations are similar in size for the numerical and experimental graphs, even though the former were constructed from a larger number of vertices. Furthermore, we show that the origin for these discrepancies are predominantly contributions from eigenstates which are localized on a fraction of bonds. For this we identify these states by exploiting the fact that, when an eigenstate is localized on a bond of which the length is varied, the associated perturbation is local and it is the only affected state, whereas if it is localized on a bond with fixed length it doesn't feel the perturbation. Accordingly, because we introduce a parametric variation which does not change the spectral density, the associated eigenvalues do not change with the parameter and thus they can be easily found. We show that the agreement with the RMT results becomes better when extracting such eigenstates. Finally, we propose a procedure which minimizes the effect of nonuniversal eigenstates. Varying the lengths of all or almost all bonds in a sufficiently complex GSE quantum graph—our example consisted of 12 vertices and 20 bonds—we were able to achieve good agreement between the numerical and RMT results for the curvature distribution and velocity correlator [55]. Note, however, that the spectral properties for a fixed parameter value still exhibit deviations since extracting eigenvalues corresponding to localized states would cause discrepancies that are due to these missing levels.

## ACKNOWLEDGMENTS

This work was supported by the NSF of China under Grants No. 11775100 and No. 11961131009. We thank Ulrich Kuhl for helping us set up the experiments with microwave networks and his valuable advise concerning the analysis of resonance spectra.

- 
- [1] T. Kottos and U. Smilansky, *Phys. Rev. Lett.* **79**, 4794 (1997).
  - [2] T. Kottos and U. Smilansky, *Ann. Phys.* **274**, 76 (1999).
  - [3] P. Pakonski, K. Życzkowski, and M. Kus, *J. Phys. A: Math. Gen.* **34**, 9303 (2001).
  - [4] C. Texier and G. Montambaux, *J. Phys. A* **34**, 10307 (2001).
  - [5] H.-J. Stöckmann, *Quantum Chaos: An Introduction* (Cambridge University Press, Cambridge, UK, 1999).
  - [6] F. Haake, *Quantum Signatures of Chaos* (Springer-Verlag, Heidelberg, 2001).
  - [7] L. Pauling, *J. Chem. Phys.* **4**, 673 (1936).
  - [8] J. A. Sánchez-Gil, V. Freilikher, I. Yurkevich, and A. A. Maradudin, *Phys. Rev. Lett.* **80**, 948 (1998).
  - [9] D. Kowal, U. Sivan, O. Entin-Wohlman, and Y. Imry, *Phys. Rev. B* **42**, 9009 (1990).
  - [10] S. Gnutzmann and A. Altland, *Phys. Rev. Lett.* **93**, 194101 (2004).
  - [11] M. L. Mehta, *Random Matrices* (Academic Press, London, 1990).
  - [12] M. Berry, *Structural Stability in Physics* (Springer, Berlin, 1979).
  - [13] G. Casati, F. Valz-Gris, and I. Guarnieri, *Lett. Nuovo Cimento* **28**, 279 (1980).
  - [14] O. Bohigas, M. J. Giannoni, and C. Schmit, *Phys. Rev. Lett.* **52**, 1 (1984).
  - [15] J. Keating, *Nonlinearity* **4**, 309 (1991).
  - [16] J. Verbaarschot, H. Weidenmüller, and M. Zirnbauer, *Phys. Rep.* **129**, 367 (1985).
  - [17] Z. Pluhař and H. A. Weidenmüller, *Phys. Rev. Lett.* **110**, 034101 (2013).
  - [18] Z. Pluhař and H. A. Weidenmüller, *Phys. Rev. E* **88**, 022902 (2013).
  - [19] Z. Pluhař and H. A. Weidenmüller, *Phys. Rev. Lett.* **112**, 144102 (2014).
  - [20] Y. V. Fyodorov, D. V. Savin, and H.-J. Sommers, *J. Phys. A* **38**, 10731 (2005).
  - [21] O. Hul, S. Bauch, P. Pakoński, N. Savytskyy, K. Życzkowski, and L. Sirko, *Phys. Rev. E* **69**, 056205 (2004).
  - [22] M. Ławniczak, S. Bauch, O. Hul, and L. Sirko, *Phys. Rev. E* **81**, 046204 (2010).
  - [23] O. Hul, M. Ławniczak, S. Bauch, A. Sawicki, M. Kuś, and L. Sirko, *Phys. Rev. Lett.* **109**, 040402 (2012).
  - [24] M. Allgaier, S. Gehler, S. Barkhofen, H.-J. Stöckmann, and U. Kuhl, *Phys. Rev. E* **89**, 022925 (2014).

- [25] M. Białous, V. Yunko, S. Bauch, M. Ławniczak, B. Dietz, and L. Sirko, *Phys. Rev. Lett.* **117**, 144101 (2016).
- [26] A. Rehemangiang, M. Allgaier, C. H. Joyner, S. Müller, M. Sieber, U. Kuhl, and H.-J. Stöckmann, *Phys. Rev. Lett.* **117**, 064101 (2016).
- [27] R. Scharf, B. Dietz, M. Kuś, F. Haake, and M. V. Berry, *Europhys. Lett.* **5**, 383 (1988).
- [28] B. Dietz, V. Yunko, M. Białous, S. Bauch, M. Ławniczak, and L. Sirko, *Phys. Rev. E* **95**, 052202 (2017).
- [29] M. Berry, *Proc. R. Soc. Lond. A* **400**, 229 (1985).
- [30] M. Sieber, U. Smilansky, S. C. Creagh, and R. G. Littlejohn, *J. Phys. A* **26**, 6217 (1993).
- [31] J. Zakrzewski and M. Kuś, *Phys. Rev. Lett.* **67**, 2749 (1991).
- [32] J. Zakrzewski and D. Delande, *Phys. Rev. E* **47**, 1650 (1993).
- [33] J. Zakrzewski, D. Delande, and M. Kuś, *Phys. Rev. E* **47**, 1665 (1993).
- [34] B. D. Simons and B. L. Altshuler, *Phys. Rev. Lett.* **70**, 4063 (1993).
- [35] B. D. Simons and B. L. Altshuler, *Phys. Rev. B* **48**, 5422 (1993).
- [36] A. Szafer and B. L. Altshuler, *Phys. Rev. Lett.* **70**, 587 (1993).
- [37] F. von Oppen, *Phys. Rev. Lett.* **73**, 798 (1994).
- [38] F. von Oppen, *Phys. Rev. E* **51**, 2647 (1995).
- [39] Y. V. Fyodorov and H.-J. Sommers, *Phys. Rev. E* **51**, R2719 (1995).
- [40] J. Zakrzewski, *Z. Phys. B* **98**, 273 (1995).
- [41] B. Dietz, M. Lombardi, and T. H. Seligman, *J. Phys. A* **29**, L95 (1996).
- [42] M. Kollmann, J. Stein, U. Stoffregen, H.-J. Stöckmann, and B. Eckhardt, *Phys. Rev. E* **49**, R1 (1994).
- [43] M. Barth, U. Kuhl, and H.-J. Stöckmann, *Phys. Rev. Lett.* **82**, 2026 (1999).
- [44] P. Bertelsen, C. Ellegaard, T. Guhr, M. Oxborrow, and K. Schaadt, *Phys. Rev. Lett.* **83**, 2171 (1999).
- [45] K. Schaadt and A. Kudrolli, *Phys. Rev. E* **60**, R3479 (1999).
- [46] Y. Hlushchuk, A. Kohler, S. Bauch, L. Sirko, R. Blümel, M. Barth, and H.-J. Stöckmann, *Phys. Rev. E* **61**, 366 (2000).
- [47] Y. Hlushchuk, U. Kuhl, and S. Russ, *Physica A* **344**, 523 (2004).
- [48] H.-J. Stöckmann, M. Barth, U. Dörr, U. Kuhl, and H. Schanze, *Physica E* **9**, 571 (2001).
- [49] B. Dietz, A. Heine, A. Richter, O. Bohigas, and P. Leboeuf, *Phys. Rev. E* **73**, 035201(R) (2006).
- [50] B. Dietz, T. Friedrich, M. Miski-Oglu, A. Richter, F. Schäfer, and T. H. Seligmann, *Phys. Rev. E* **80**, 036212 (2009).
- [51] B. Dietz and A. Richter, *Chaos* **25**, 097601 (2015).
- [52] M. Ławniczak, A. Borkowska, O. Hul, S. Bauch, and L. Sirko, *Act. Phys. Pol. A* **120**, A-185 (2011).
- [53] M. Ławniczak, A. Nicolau-Kuklińska, O. Hul, P. Masiak, S. Bauch, and L. Sirko, *Phys. Scr.* **T153**, 014041 (2013).
- [54] O. Hul, P. Šeba, and L. Sirko, *Phys. Rev. E* **79**, 066204 (2009).
- [55] O. Hul, P. Šeba, and L. Sirko, *Phys. Scr.* **T135**, 014048 (2009).
- [56] O. Hul and L. Sirko, *Phys. Rev. E* **83**, 066204 (2011).
- [57] D. S. Jones, *Theory of Electromagnetism* (Pergamon, Oxford, UK, 1964).
- [58] N. Savvitsky, A. Kohler, S. Bauch, R. Blümel, and L. Sirko, *Phys. Rev. E* **64**, 036211 (2001).
- [59] O. Bohigas, R. U. Haq, and A. Pandey, *Nuclear Data for Science and Technology* (Reidel, Dordrecht, 1983).
- [60] H.-J. Stöckmann and J. Stein, *Phys. Rev. Lett.* **64**, 2215 (1990).
- [61] S. Sridhar, *Phys. Rev. Lett.* **67**, 785 (1991).
- [62] H.-D. Gräf, H. L. Harney, H. Lengeler, C. H. Lewenkopf, C. Rangacharyulu, A. Richter, P. Schardt, and H. A. Weidenmüller, *Phys. Rev. Lett.* **69**, 1296 (1992).
- [63] P. So, S. M. Anlage, E. Ott, and R. N. Oerter, *Phys. Rev. Lett.* **74**, 2662 (1995).
- [64] T. Kottos and U. Smilansky, *J. Phys. A* **36**, 3501 (2003).
- [65] P. Lebœuf and M. Sieber, *Phys. Rev. E* **60**, 3969 (1999).
- [66] B. Dietz, M. Lombardi, and T. H. Seligman, *Ann. Phys.* **312**, 441 (2004).
- [67] B. Dietz, A. Heine, V. Heuveline, and A. Richter, *Phys. Rev. E* **71**, 026703 (2005).
- [68] C. Poli, B. Dietz, O. Legrand, F. Mortessagne, and A. Richter, *Phys. Rev. E* **80**, 035204(R) (2009).